General Disclaimer

One or more of the Following Statements may affect this Document

- This document has been reproduced from the best copy furnished by the organizational source. It is being released in the interest of making available as much information as possible.

- This document may contain data, which exceeds the sheet parameters. It was furnished in this condition by the organizational source and is the best copy available.

- This document may contain tone-on-tone or color graphs, charts and/or pictures, which have been reproduced in black and white.

- This document is paginated as submitted by the original source.

- Portions of this document are not fully legible due to the historical nature of some of the material. However, it is the best reproduction available from the original submission.

OLD DOMINION UNIVERSITY RESEARCH FOUNDATION

SCHOOL OF ENGINEERING
OLD DOMINION UNIVERSITY
NORFOLK, VIRGINIA

Technical Report 75-T16

A GENERAL ALGORITHM USING FINITE ELEMENT METHOD FOR AERODYNAMIC CONFIGURATIONS AT LOW SPEEDS

By

R. Balasubramanian

Final Report

Prepared for the
National Aeronautics and Space Administration
Langley Research Center
Hampton, Virginia

Under
Grant NSG 1094
August 6, 1974 - August 25, 1975

November 1975

TABLE OF CONTENTS

A GENERAL ALGORITHM USING FINITE ELEMENT METHOD FOR AERODYNAMIC CONFIGURATIONS AT LOW SPEEDS

By

R. Balasubramanian[1]

SUMMARY

A finite element algorithm for numerical simulation of two-dimensional, incompressible, viscous flows has been developed. The Navier-Stokes equations are suitably modelled to facilitate direct solution for the essential flow parameters. A leap-frog time differencing and Galerkin minimization of these model equations yields the finite element algorithm. The finite elements are triangular with bicubic shape functions approximating the solution space. The finite element matrices are unsymmetrically banded to facilitate savings in storage. An unsymmetric L-U decomposition is performed on the finite element matrices to obtain the solution for the boundary value problem.

INTRODUCTION

Under grant NSG-1094, a computer program for numerical solution of two-dimensional, incompressible, viscous flows has been developed. The program is operational and has been used to simulate the "driven cavity" problem. The numerical results for the "driven cavity" are compared with known finite difference solutions. The purpose of this report is to provide documentation of the preliminary numerical results as well as to present the software programs generated under grant NSG-1094.

The Analytical Fluid Mechanics Section, FMB, HSAD, LaRC has been in the process of evaluating the efficiency of finite element

---

[1] Research Associate, Old Dominion University, Norfolk, Virginia 23508.

techniques for fluid problems. An algorithm for high speed flows was previously under development (ref. 1) when the author proposed low speed simulation studies in 1974. The results of the present investigation indicate that further research should be completed in order to obtain objective comparisons. The research effort of the author was, however, redirected to enable him to participate in research work on "compliant walls". It is hoped that further extensions of the present work will be undertaken at a later date.

THE FINITE ELEMENT METHOD

The finite element method has been used with a great deal of success as a simulation technique for problems in structural mechanics. There are excellent books (refs. 2, 3) which detail the general capabilities of the method and its applications. However, there have been only a few known successful applications of this technique to fluid flow problems. Even in those cases that are reported in the literature no rigorous comparison has been made between the finite element and finite difference solutions for the same test problem of accuracy, efficiency, cost, or storage. It is felt that such a comparison should be made; hence, the test problem of driven cavity has been undertaken where extensive finite difference solutions are available (ref. 4).

Traditionally, the problems in fluid dynamics have been studied by using the "high speed variables" (primitive variables: u, v, ρ) for supersonic flows and by using the "low-speed variables" (streamfunction-vorticity: Ψ, ζ) for subsonic flows. In recent years, where mixed flows have had to be analyzed it has become imperative to develop numerical techniques where flow variables can be used at all speeds. In the literature are found the MAC, SMAC, ICE methods and Chorin's artificial compressibility method (refs. 5, 6, 7, and 8), primarily for such applications. The Fluid Mechanics Branch was also motivated to develop a primitive variables algorithm from such a consideration.

One of the major problems associated with incompressible flows is the solution of the continuity equation (hence the concept of stream-functions and stream tubes). When primitive variables are used, the continuity equation has to be satisfied through some iteration procedure. A natural parameter for iteration is the pressure. In this report two different schemes of iteration, which will be referred to in subsequent sections of this report as Models I and II, have been used. Some of the more important features of the present algorithm may be summarized as follows:

- Triangular finite elements with bicubic shape functions (T-10 element) (ref. 9). Order of accuracy $O(h^4)$ in space.
- Leap-frog differencing for marching to steady state (Crank-Nicholson scheme). Order of accuracy $O(t^2)$ in time.
- Guyan reduction to eliminate "unnecessary" degrees of freedom.
- A special Poisson solver for elliptic problems which conserves the basic conservation laws, thereby improving overall accuracy of the finite elements.

Fluid Dynamic Equations

The governing equations for two-dimensional, incompressible, viscous flow in a rectangular coordinate system are as follows:

$$\frac{\partial \bar{u}}{\partial x} + \frac{\partial \bar{v}}{\partial y} = 0 \tag{1a}$$

$$\frac{\partial \bar{u}}{\partial t} + \bar{u}\frac{\partial \bar{u}}{\partial x} + v\frac{\partial \bar{u}}{\partial y} = -\frac{1}{\rho}\frac{\partial \bar{p}}{\partial x} \cdot \frac{1}{\zeta} + \nu\left(\frac{\partial^2 \bar{u}}{\partial x^2} + \frac{\partial^2 \bar{u}}{\partial y^2}\right) \tag{1b}$$

$$\frac{\partial \bar{v}}{\partial t} + \bar{u}\frac{\partial \bar{v}}{\partial x} + v\frac{\partial \bar{v}}{\partial y} = -\frac{1}{\rho} \cdot \frac{\partial \bar{p}}{\partial y} + \nu\left(\frac{\partial^2 \bar{v}}{\partial x^2} + \frac{\partial^2 \bar{v}}{\partial y^2}\right) \tag{1c}$$

where, $\bar{u}$ is the velocity in the x-direction, $\bar{v}$ is the velocity in the y-direction, and $\bar{p}$ is the pressure.

Non-dimensionalize the flow equations using the diffusion scales, i.e.,

$$\tau = \frac{Ut}{L} \tag{2a}$$

$$\xi = \frac{x}{L}\ ,\quad \eta = \frac{y}{L} \tag{2b}$$

$$u = \frac{\bar{u}}{U} \tag{2c}$$

$$v = \frac{\bar{v}}{U} \tag{2d}$$

$$p = \frac{\bar{p}}{\rho U^2}\ . \tag{2e}$$

The non-dimensional Reynolds number is defined as

$$Re = \frac{UL}{\nu}\ . \tag{3}$$

Equations (1a, b, c) in non-dimensional form are

$$\frac{\partial u}{\partial \xi} + \frac{\partial v}{\partial \eta} = 0 \tag{4a}$$

$$\frac{\partial u}{\partial \tau} + u\frac{\partial u}{\partial \xi} + v\frac{\partial u}{\partial \eta} = -\frac{\partial p}{\partial \xi} + \frac{1}{Re}\left(\frac{\partial^2 u}{\partial \xi^2} + \frac{\partial^2 u}{\partial \eta^2}\right) \tag{4b}$$

$$\frac{\partial v}{\partial \tau} + \bar{u}\frac{\partial v}{\partial \xi} + \bar{v}\frac{\partial v}{\partial \eta} = -\frac{\partial p}{\partial \eta} + \frac{1}{Re}\left(\frac{\partial^2 v}{\partial \xi^2} + \frac{\partial^2 v}{\partial \eta^2}\right)\ . \tag{4c}$$

Iteration Schemes

The system of equations (4a) to (4c) is not amenable to direct solution because of the nature of the incompressibility condition of equation (4a). Described below are two different models for the equations (4a, b, c).

Model I

$$\frac{\partial p}{\partial \tau} + Kp\left(\frac{\partial u}{\partial \xi} + \frac{\partial v}{\partial \eta}\right) = 0 \tag{5a}$$

$$\frac{\partial u}{\partial \tau} + u\frac{\partial u}{\partial \xi} + v\frac{\partial u}{\partial \eta} = -\frac{\partial p}{\partial \xi} + \frac{1}{Re}\left(\frac{\partial^2 u}{\partial \xi^2} + \frac{\partial^2 u}{\partial \eta^2}\right) \tag{5b}$$

$$\frac{\partial v}{\partial \tau} + u\frac{\partial v}{\partial \xi} + v\frac{\partial v}{\partial \eta} = -\frac{\partial p}{\partial \eta} + \frac{1}{Re}\left(\frac{\partial^2 v}{\partial \xi^2} + \frac{\partial^2 v}{\partial \eta^2}\right) \qquad (5c)$$

where K is an artificially chosen time parameter. Equations (5a, b, c) describe a purely hyperbolic system when the viscous terms are absent and can, hence, be viewed as hyperbolic for fairly large Reynolds number flows (see Appendix A). The incompressibility condition as modelled by Equation (5a) is a restatement, at steady state, $\left(\text{i.e., } t \to \infty \; ; \; \frac{\partial p}{\partial \tau} \to 0\right)$ that the work done by the pressure forces is equal to zero. Model I was tested on the driven cavity problem. It was observed that the artificial time constant "K" can be chosen to accelerate or decelerate the march to steady state. A careful choice of "K" is essential to successfully implement this algorithm. At high Reynolds numbers oscillations were seen, as a direct result of ill-chosen values for "K".

Model II

$$\frac{\partial u^*}{\partial \tau} + u\frac{\partial u^*}{\partial \xi} + v\frac{\partial u^*}{\partial \eta} = -\frac{\partial p}{\partial \xi} + \frac{1}{Re}\left(\frac{\partial^2 u^*}{\partial \xi^2} + \frac{\partial^2 u^*}{\partial \eta^2}\right) \qquad (6a)$$

$$\frac{\partial v^*}{\partial \tau} + u\frac{\partial v^*}{\partial \xi} + v\frac{\partial v^*}{\partial \eta} = -\frac{\partial p}{\partial \eta} + \frac{1}{Re}\left(\frac{\partial^2 v^*}{\partial \xi^2} + \frac{\partial^2 v^*}{\partial \eta^2}\right) \qquad (6b)$$

$$\frac{\partial^2 p}{\partial \xi^2} + \frac{\partial^2 p}{\partial \eta^2} = \frac{\partial u^*}{\partial \xi} + \frac{\partial v^*}{\partial \eta} \qquad (6c)$$

$$u = u^* - \frac{\partial p}{\partial \xi} \qquad (6d)$$

$$v = v^* - \frac{\partial p}{\partial \eta} \qquad (6e)$$

The model equations (6) follow from the SMAC methodology (ref. 5). The Navier-Stokes equations are solved (6a, b) to obtain an auxiliary field (u*, v*); the pressure gradients appearing in equation (6a, b) are pseudo-pressure gradients. The pseudo-pressure is obtained by solving a Poisson equation (6c). The actual velocity fields are obtained by applying corrections (6d, e). The model is valid whenever velocity-splitting is justifiable. Assuming that this is so, we notice equations (6d, e)

$$u = u^* - \nabla p$$

and hence,

$$\nabla \cdot u = \nabla \cdot u^* - \nabla \cdot \nabla \cdot p \tag{7a}$$

By forcing

$$\nabla \cdot u = 0 \tag{7b}$$

one obtains (6c) i.e.,

$$\nabla \cdot \nabla p = \nabla \cdot u^* \tag{7c}$$

This model was also tested on the driven cavity problem. A special Poisson solver, using a variational formulation (Weak-Galerkin method) with undetermined Lagrangian multipliers, was developed to solve the Poisson equation (6c) when it was found that conventional finite element method of satisfying the boundary conditions for this problem violated the basic conservation laws on the boundary. For details, see reference (10).

Finite Element Algorithm

Triangular elements with bicubic basis functions ϕ_J (J = 1, 2, . . . 10) associated with triangles are chosen in this work (Appendix B). The basis functions have support only on the triangulation. A leap-frog differencing scheme is used on the model equations to yield an implicit procedure. Equation system (5a, b, c) after differencing can be written as follows:

$$\frac{u^* - u^{n-1}}{2\tau} + \frac{u^n}{2}(u^*,x + u^{n-1},x) + \frac{v^n}{2}(u^*,y + u^{n-1},y) + p^n,x$$

$$= \frac{1}{2R}(u^*,x + u^{n-1},x),x - \frac{1}{2R}(u^*,y + u^{n-1},y),y$$

$$= L_1(u^*) \tag{8a}$$

$$\frac{v^* - v^{n-1}}{2\tau} + \frac{u^n}{2}(v^*,x + v^{n-1},x) + \frac{v^n}{2}(v^*,y + v^{n-1},y) + p^n,y$$

$$- \frac{1}{2R}(v^*,x + v^{n-1},x),x - \frac{1}{2R}(v^*,y + v^{n-1},y),y$$

$$= L_2(v^*) \qquad (8b)$$

$$\frac{p^* - p^{n-1}}{2\tau} + \frac{kp^n}{2}(u^*,x + u^{n-1},x + v^*,y + v^{n-1},y) = L_3(p^*) \qquad (8c)$$

where u^*, v^*, p^* are the current variables, L_1, L_2, L_3 are the "residuals", the superscripts (n) and (n - 1) refer to previous time periods and commas (,) indicate partial differentials.

It should be noted that the current variables u^*, v^*, p^* can be expressed in terms of the nodal variables $\hat{u}_j$, $\hat{v}_j$, $\hat{p}_j$ (j = 1, 2, . . . 10) as,

$$u^* = \sum_j \phi_j \hat{u}_j = \{\phi\}^T\{\hat{u}\} \qquad (9a)$$

$$v^* = \sum_j \phi_j \hat{v}_j = \{\phi\}^T\{\hat{v}\} \qquad (9b)$$

$$p^* = \sum_j \phi_j \hat{p}_j = \{\phi\}^T\{\hat{p}\} \qquad (9c)$$

The finite element algorithm is obtained by minimization of the residuals in equation (8) by the weights ϕ_j (j = 1, 2, . . . 10) (Galerkin method), thus yielding 30 equations in 30 unknowns ($\hat{u}$, $\hat{v}$, $\hat{p}$). Expansions such as 9a, b, c are used to describe the fields at "n" and "(n - 1)", i.e.,

$$p^n = \{\phi\}^T\{\hat{p}\}^n$$

$$p^{n-1} = \{\phi\}^T\{\hat{p}\}^{n-1} \quad \text{etc.} \qquad (10)$$

After manipulations, the set of algebraic equations

$$[A^1]\{\hat{p}\} = \{b_1\} ,$$

$$[A^2]\{\hat{u}\} = \{b_2\} , \qquad (11)$$

$$[A^2]\{\hat{v}\} = \{b_3\} .$$

are obtained, where $[A^1], [A^2]$ are square matrices (10 10), called the element stiffness matrices, $\{b_1\}$, $\{b_2\}$, $\{b_3\}$ are "load vectors" (10 × 1). Details of the derivation of the stiffness matrix and load vector are given in Appendix C.

Note that

$$A^1{}_{i,j} = \left[\iint_\Omega \phi_i\phi_j d\Omega + K\tau \iint_\Omega \sum_k \left\{<\phi_{k,x}u_k> + <\phi_{k,y}v_k>\right\} \phi_i\phi_j d\Omega\right] \qquad (12a)$$

$$A^2{}_{i,j} = \left[\iint_\Omega \phi_i\phi_j d\Omega + \tau \iint_\Omega \sum_k \left\{<\phi_k u_k{}^n> \phi_{i,x}\phi_j + <\phi_k v_k{}^n> \phi_{i,x}\phi_j\right\} d\Omega\right.$$

$$+ \frac{\tau}{R} \iint_\Omega \left\{\phi_{i,x}\phi_{j,x} + \phi_{i,y}\phi_{j,y}\right\} d\Omega$$

$$\left. + \frac{\tau}{R} \int_\Gamma (\phi_j\phi_{i,y}dx - \phi_j\phi_{i,x}dy)\right] \qquad (12b)$$

$$b^1{}_j = \iint_\Omega <\phi_i p_i{}^n> \phi_j d\Omega - K\tau \iint_\Omega \sum_k <\phi_{k,x}u_k>$$

$$\left. + <\phi_{k,y}v_k>\right\} <\phi_i p^n> \phi_j d\Omega \qquad (12c)$$

$$b^2{}_j = \iint_\Omega <\phi_i u_i{}^{n-1}> \phi_j d\Omega - \tau \iint_\Omega \sum_k \left\{<\phi_k u_k{}^n> <\phi_{i,x}u_i{}^{n-1}>\right.$$

$$\left. + <\phi_k v_k{}^n> <\phi_{i,y}u_i{}^{n-1}>\right\} \phi_j d\Omega$$

$$- \frac{\tau}{R} \iint_\Omega \left\{<\phi_{i,x}u_i{}^{n-1}> \phi_{j,x} + <\phi_{i,y}u_i{}^{n-1}> \phi_{j,y}\right\} d\Omega$$

$$- \frac{\tau}{R} \int_\Gamma (<\phi_{i,y}u_i{}^{n-1}> \phi_j d_x - <\phi_{i,x}u_i{}^{n-1}> \phi_j dy)$$

$$+ 2\tau \iint_{\Omega} \langle \phi_i p_i^n \rangle \phi_{j,x} d\Omega - 2\tau \int_{\Gamma} \langle \phi_i p_i^n \rangle \phi_j dy \qquad (12d)$$

$$b^3_j = \iint_{\Omega} \langle \phi_i v_i^{n-1} \rangle \phi_j d\Omega - \tau \iint_{\Omega} \sum_k \left\{ \langle \phi_k u_k^n \rangle \langle \phi_{i,x} v_i^{n-1} \rangle + \langle \phi_k v_k^n \rangle \langle \phi_{i,y} v_i^{n-1} \rangle \right\} \phi_j d\Omega$$

$$- \frac{\tau}{R} \iint_{\Omega} \left\{ \langle \phi_{i,x} v_i^{n-1} \rangle \phi_{j,x} + \langle \phi_{i,y} v_i^{n-1} \rangle \phi_{j,y} \right\} d\Omega$$

$$- \frac{\tau}{R} \int_{\Gamma} \left\{ \langle \phi_{i,y} v_i^{n-1} \rangle \phi_j dx - \langle \phi_{i,x} v_i^{n-1} \rangle \phi_j dy \right\}$$

$$+ 2\tau \iint_{\Omega} \left\{ \langle \phi_i p_i^n \rangle \phi_{j,y} d\Omega + 2\tau \int_{\Gamma} \langle \phi_i p_i^n \rangle \phi_j dx \right\} \qquad (12e)$$

It should be noted that the element stiffness matrices for u, v have identical form, thus saving one assembly. The various integrations are done with quadrature schemes. The 16 point scheme of Hammer, Marlow and Stroud (11) accurate to total degree five, is used for area integrals. A third order Gaussian quadrature is used for line integrals. To perform integrations the finite element triangulation is transformed to a standard triangle whose coordinates are (0, 0; +1, -1; +1, +1) through linear mapping T. Before any global assembly the stiffness matrices are transformed to the global values through the relation

$$[K_g] = [T]^T [K][T] \qquad (13)$$

Guyan Reduction

The internal degree of freedom is often cumbersome to carry, incurring penalty in storage by way of increased bandwidth and increased number of equations. A Guyan reduction (9) is carried out to eliminate the internal degrees of freedom to obtain compact (9 × 9) element stiffness matrices.

Program Documentation

To obtain the solution of a boundary value problem, the following informations needs to be input to the finite element

program:

1. The topology of the finite element space i.e., number of elements, nodes, details of connectivity, flags for boundary integrals indicating the orientation of the boundary etc.,

2. The initial and boundary conditions, and

3. Quadrature weights.

A mesh generator was developed to create information on finite element topology, thereby reducing the cumbersome job of hand-inputting. Figure 1a, b shows the finite element discretisation obtained by using the mesh generator. Presently, the mesh generator can be used only for discretisation of regular geometries; however, extensions to irregular domains can be achieved by slight modifications in the code. The discretisation obtained is uniform. The mesh generator requires a minimum number of data cards and creates a massive amount of data for the main program. Figure 1 was obtained by specifying $a = 1$, $b = 1$, $d = 1/5$, and for Figure 2 set $a = 1$, $b = 1$, $d = 1/9$ where a and b are the dimensions of the rectangular domain and d is the mesh width.

For functional efficiency the finite element package developed was partitioned into two separate program segments. In Part I a new geometry and a new discretisation are processed and the output of this program consisting of quadrature values of spline function, matrix structure of the finite element matrices, flags for boundary integrals, etc. is saved. In Part II, for the given topology and boundary and initial conditions, finite element solutions are generated at each time level. All matrix operations are performed in Part II. The components that go into this program are 1) stiffness matrix assembler (to assemble element contributions into a global assembly), 2) an L-U decomposition routine (where a matrix is decomposed into upper and lower triangular components), 3) a matrix routine which converts a given matrix in local coordinate systems into a global matrix.

While developing the algorithm an attempt was made to exploit the known sparse structure of the finite element matrices, thereby enhancing savings in storage.

Numerical Results for the Test Problem

The test problem considered is a driven cavity. The upper wall, Figure 3, moves with uniform velocity $\bar{u} = 1$ for $t > 0$. Finite element solutions were obtained using Models I and II (see "Iteration Schemes," pages 4 and 5). At the Reynolds numbers that were considered (R = 1, 10) both models behaved very well. Tables 1 to 6 show the converged finite element fields (9 × 9 mesh) and the converged finite difference (17 × 17 mesh) solutions, for Re = 1.0 (Model II solutions). The finite difference solutions were computed using an ADI algorithm developed by Morris (ref. 12) Figure 4 shows the velocity profiles through the vortex center.

Finite element approximations should show uniform convergence with decreasing mesh size.* To study the effect of discretization of solution, two finite element meshes (5 × 5, fig. 1, and 9 × 9, fig. 2) were run. The 5 × 5 mesh could not capture all the details of the flow as was expected although the correct trend for flow variables was observable. (The vorticity value at the top moving wall at the point midway between the corners was 3.9 at Re = 1.0, rather low and at the point away from the singularity 9.8; again a low value.) The 9 × 9 mesh compared favorably to a 17 × 17 finite difference grid as can be seen from Tables 1 to 6; and was superior to 9 × 9 finite difference solutions. This was anticipated since theoretical considerations show the finite element solutions to have an $O(h^4)$ accuracy compared to the second order accurate ADI method. However, the finite element solutions could not reproduce the fourth order accuracy. This was due to the fact that when using the finite element algorithm on the driven cavity, the boundary conditions at the singular points A and B (fig. 2) had to be modelled In finite difference methods the nature of differencing leaves the singular points alone.) With special singular function expansions, these singularities can be correctly modelled in finite element methods. The next logical step in the numerical simulation will be

* The Tocher-10 model gives piecewise continuous first derivatives in the interelement boundaries and hence exemplifies a non-conforming element. For these elements uniform convergence as mesh sizes goes to zero is not always guaranteed.

to use the singular function expansions. Even the results that have been obtained through an ad-hoc modelling of the singular points (Tables 1-6) indicate that the finite elements can capture singularities far better than finite difference techniques. For instance, comparison of the vorticities on the vertical walls (Tables 5 and 6) indicate the correct behavior near the singularity in the finite element solution that the finite difference solutions are unable to predict. This point is emphasized with the following logic: If one were to go along the moving wall towards the singularity the vorticity at the singularity would be $+\infty$; along the vertical wall, though, the vorticity has to be negative to exhibit the driven nature of the flow. The corner points at the bottom should have zero vorticity from consideration of continuity of derivatives in either direction. The point on the wall closest to the singular point A (see fig. 3) does not therefore have the largest negative value of vorticity. (Since the vorticity field has to go to zero at the bottom point, has a negative maximum on the wall, and must reach $+\infty$ at the singular point, the only way this behavior can be exhibited by a continuous field is to have a negative maximum vorticity farther down). So far, to the author's knowledge no finite difference solution has indicated this behavior around the singular point.

CONCLUSIONS

A finite element algorithm for low speeds has been developed. The algorithm, applied to driven cavity problem, produced numerical results which were in good comparison with finite-difference results. Further research in this area is required in order to obtain conclusive results regarding the efficiency of the current algorithm as compared to other current solution techniques such as finite difference procedures.

Table 1. Finite element solution (9 × 9 mesh) for velocity component u. Re. No. = 1.0, converged velocity field.

y \ x →	0	0.125	0.25	0.375	0.5	0.625	0.75	0.875	1.0
1.0	0	1.0	1.0	1.0	1.0	1.0	1.0	1.0	0
0.875	0	.1158	0.2500	.3151	.3820	.3156	.2569	0.1189	0
0.75	0	.0013	-0.0810	-0.0386	-0.0227	-0.0377	-0.0794	0.0011	0
0.625	0	-0.0573	-0.1222	- .1698	- .1881	-0.1708	- .1233	-0.0579	0
0.5	0	-0.0446	-0.1222	- .1953	- .2000	-0.1964	-0.1230	-0.0449	0
0.375	0	-0.0482	-0.1085	-0.1491	-0.1849	-0.1495	-0.1094	-0.0485	0
0.25	0	-0.0256	-0.0752	-0.1188	- .1303	- .1191	-0.0756	-0.0258	0
0.125	0	-0.0117	-0.0427	-0.0715	-0.0797	-0.0717	-0.0430	-0.0119	0
0	0	0	0	0	0	0	0	0	0

Table 2. Finite difference solution (17 × 17 mesh) for velocity component u (ref. 12). Converged solution.

↓ y \ x →	0	.125	0.25	0.375	0.5	0.625	0.75	0.875	1.0
1.0	0	1.0	1.0	1.0	1.0	1.0	1.0	1.0	0
0.875	0	0.0195	0.2004	0.3221	0.3619	0.3246	0.2042	0.0212	0
0.75	0	-0.0817	-0.0830	-0.0408	-0.0204	-0.0406	- .0837	-0.0833	0
0.625	0	-0.0687	-0.1407	- .1695	- .1755	- .1708	- .1429	-0.0702	0
0.5	0	-0.0503	-0.1287	- .1820	- .2000	- .1832	- .1302	-0.0511	0
0.375	0	-0.0353	-0.0995	- .1508	- .1698	- .1513	- .1001	-0.0356	0
0.25	0	-0.0229	-0.0682	- .1078	- .1231	- .1079	- .0684	-0.0229	0
0.125	0	-0.0109	-0.0364	-0.0605	-0.0702	-0.0606	-0.0364	-0.0108	0
0.0	0	0	0	0	0	0	0	0	0

Table 3. Finite element solution (9 × 9 mesh) for velocity component v . Re. No. = 1.0, converged solution.

↓y \ x→	0.0	0.125	0.25	0.375	0.5	0.625	0.75	0.875	1.0
1.0	0	0	0	0	0	0	0	0	0
0.875	0	0.2779	0.0870	0.0313	0.0010	-0.0295	-0.0859	-0.2778	0
0.75	0	0.3160	0.2497	0.1139	0.0015	-0.1104	-0.2502	-0.3214	0
0.625	0	0.2211	0.2104	0.1385	0.0018	-0.1370	-0.2114	-0.2230	0
0.5	0	0.1347	0.1640	0.0891	0.0007	-0.0880	-0.1641	-0.1353	0
0.375	0	0.0882	0.0927	0.0680	0.0004	-0.0674	-0.0924	-0.0885	0
0.25	0	0.0441	0.0610	0.0361	0.0002	-0.0359	-0.0610	-0.0441	0
0.125	0	0.0192	0.0211	0.0151	0.00	-0.0151	-0.0211	-0.0192	0
0.0	0	0	0	0	0	0	0	0	0

Table 4. Finite difference solution (17 × 17 mesh) for velocity component v (ref. 12). Re. No. = 1.0, converged solution.

↓ y \ x →	0.0	0.125	0.25	0.375	0.5	0.625	0.75	0.875	1.0
1.0	0	0	0	0	0	0	0	0	0
0.875	0	0.2977	0.1571	0.0618	0.0009	-0.0598	-0.1557	-0.2999	0
0.75	0	0.3132	0.2560	0.1267	0.0018	-0.1238	-0.2558	-0.3168	0
0.625	0	0.2343	0.2374	0.1342	0.0015	-0.1322	-0.2380	-0.2366	0
0.5	0	0.1522	0.1730	0.1056	0.0007	-0.1048	-0.1735	-0.1531	0
0.375	0	0.0865	0.1059	0.0679	0.0003	-0.0676	-0.1062	-0.0867	0
0.25	0	0.0394	0.0520	0.0346	0.0001	-0.0346	-0.0521	-0.0394	0
0.125	0	0.0103	0.0155	0.0107	0.0	-0.0107	-0.0155	-0.104	0
0.0	0	0	0	0	0	0	0	0	0

Table 5. Finite element solution (9 × 9) of the vorticity field, Re. No. = 1.0, converged solution.

y \ x	0.0	0.125	0.25	0.375	0.5	0.625	0.75	0.875	1.0
1.0	18.016	19.811	10.936	7.162	5.115	7.164	10.840	19.833	18.185
0.875	-2.739	7.150	5.109	5.030	4.514	5.041	5.105	7.287	-2.767
0.75	-6.758	0.30133	2.3280	2.366	1.763	2.391	2.391	0.351	-6.893
0.625	-2.144	0.194456	0.819	1.205	1.348	1.231	0.854	0.175	-2.194
0.5	-1.208	-0.401	0.573	0.569	0.747	0.572	0.569	-0.408	-1.219
0.375	-1.317	-0.579	-0.032	0.400	0.274	0.399	-0.034	-0.579	-1.323
0.25	-0.454	-0.369	-0.205	-0.043	0.114	-0.043	-0.205	-0.370	-0.453
0.125	-0.225	-0.290	-0.276	-0.278	-0.344	-0.278	-0.277	-0.292	-0.224
0.0	0.0	-0.089	-0.459	-0.749	-0.997	-0.752	-0.463	-0.091	0.0

Table 6. Finite difference solution (17 × 17 mesh) of the vorticity field (ref. 12); Re. No. = 1.0, converged solution.

↓ y \ x →	0.0	0.125	0.25	0.375	0.5	0.625	0.75	0.875	1.0
1.0	*	15.926	8.895	6.497	5.884	6.461	8.802	15.774	*
0.875	-8.319	3.195	4.878	4.728	4.594	4.734	4.920	3.287	-8.460
0.75	-5.060	-0.362	1.988	2.799	2.989	2.832	2.047	-0.336	-5.145
0.625	-3.010	-0.924	0.627	1.427	1.669	1.447	0.649	-0.930	-3.042
0.5	-1.744	-0.794	0.069	0.605	0.783	0.610	0.070	-0.803	-1.751
0.375	-0.909	-0.544	-0.139	0.145	0.244	0.145	-0.143	-0.550	-0.908
0.25	-0.361	-0.328	-0.216	-0.126	-0.094	-0.127	-0.218	-0.330	-0.359
0.125	-0.053	-0.182	-0.265	-0.336	-0.365	-0.336	-0.265	-0.182	-0.052
0.0	0.0	-0.055	-0.317	-0.589	-0.700	-0.589	-0.319	-0.054	0.0

* Not computed.

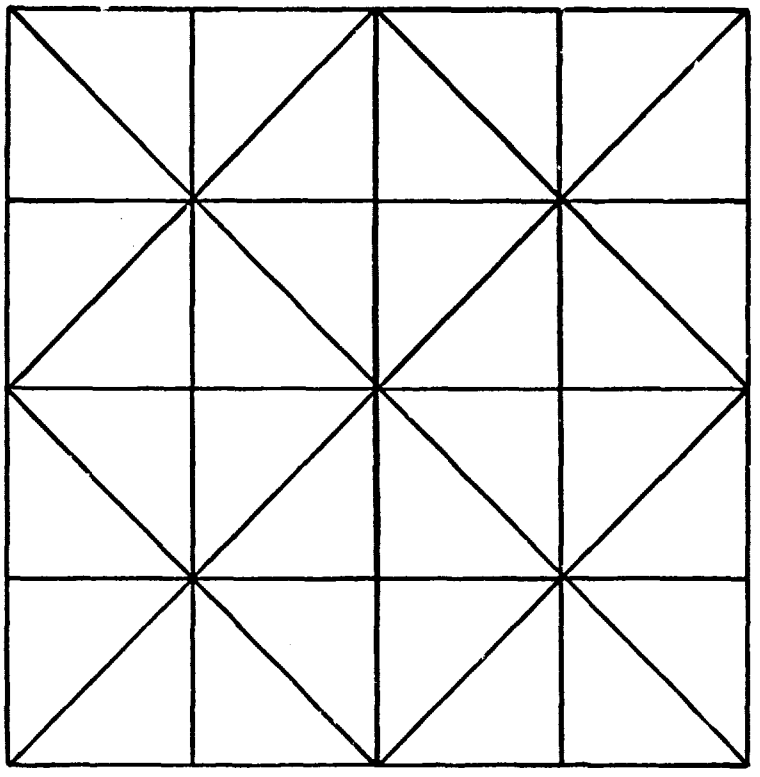

Figure 1. 5 × 5 finite element mesh obtained from the mesh generator.

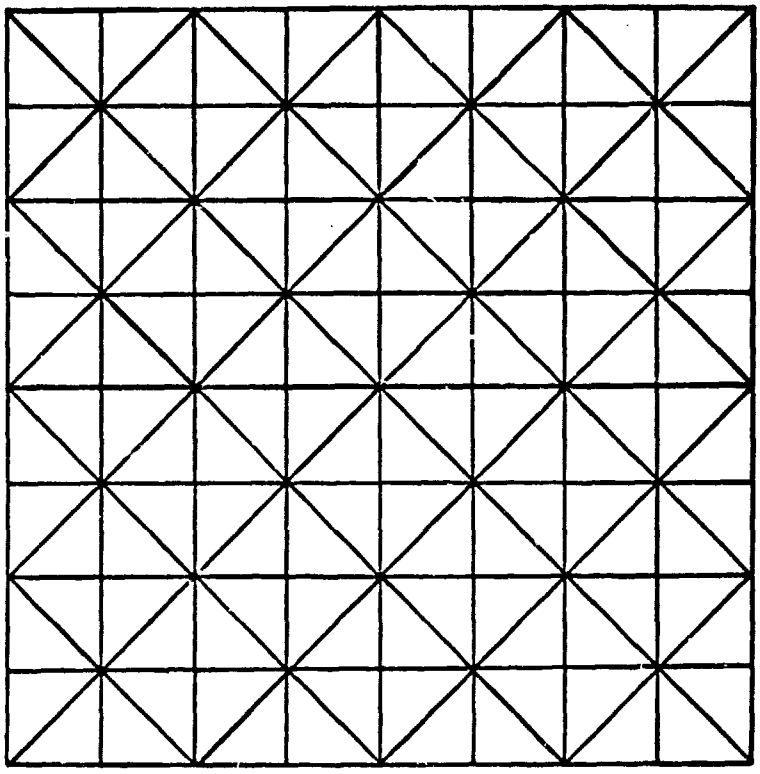

Figure 2. 9 × 9 finite element mesh obtained from the mesh generator.

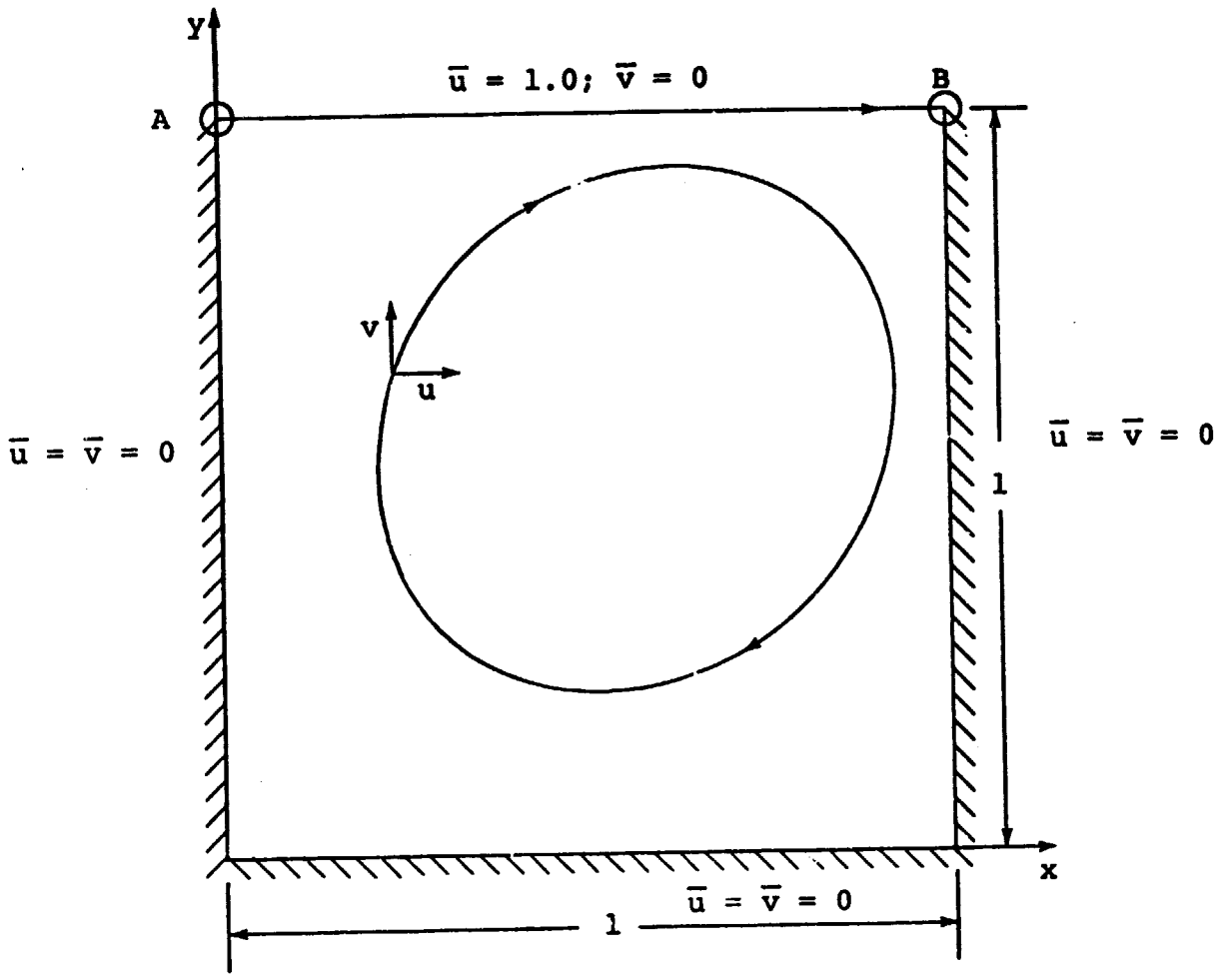

Figure 3. Schematic of the driven cavity problem.

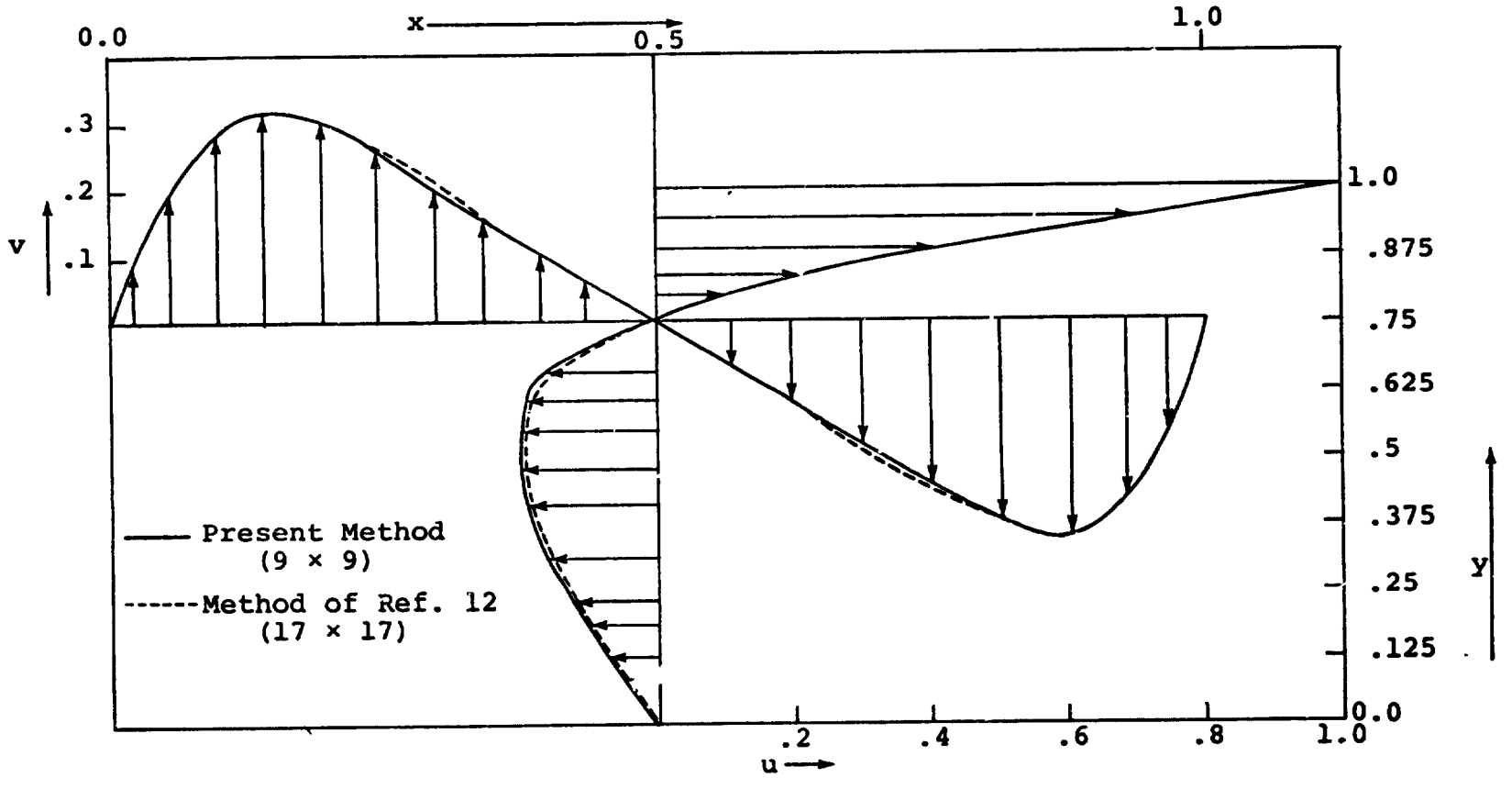

Figure 4. u, v profiles through center of vortex for square cavity.

REFERENCES

1. Cooke, C. H. and D. K. Blanchard. "Finite Element Solution of a High Speed Jet Mixing Problem for the Viscous Compressible Navier-Stokes Equations," School of Engineering, School of Engineering, Old Dominion University, Norfolk, VA Feb 1975.

2. Zienkiewicz, O. C. "The Finite Element Method in Engineering Science," McGraw-Hill, 1971.

3. Norrie, D. H. and G. DeVries. "The Finite Element Method," Academic Press 1973.

4. Numerical Studies of Incompressible Viscous Flow in a Driven Cavity; NASA-SP-378, 1975.

5. Harlow, G. H. and Welch, J. E. "Numerical Study of Large Amplitude Free Surface Motions," Physics of Fluids, Vol. 9, pp. 842-851 (1966).

6. Amsden, A. A. and Harlow, F. H. "A Simplified MAC Technique for Incompressible Fluid Flow Calculations, J. of Comp. Phys., Vol. 6, pp. 322- 325, 1970.

7. Harlow, F. H. and Amsden, A. A. "A Numerical Fluid Dynamics Method for all Flow Speeds ," J. Comp. Phys, Vol. 8, pp. 197-213, 1971.

8. Chorin, A. J. "A Numerical Method for Solving Incompressible Viscous Flow Problems," J. of Comp. Phys., Vol. 2, pp. 12-26, 1967.

9. Balasubramanian, R. "An Iterative Finite Element Method for Viscous Flow," MS Thesis, Univ. of Calgary, Alta. Canada, Feb 1974.

10. Fix, G. J. "Finite Elements and Fluid Dynamics," Rep. no. 75-1, ICASE, LaRC, Hampton, VA, 1975.

11. Hammer, P. C., O. P. Marlowe, and A. H. Stroud. "Numerical Integration over Simplexes and Cones," Math Tables Aids. Comp., 10, 130-137, 1957.

12. Morris, D. J. In "Numerical Studies of Incompressible Viscous Flow in a Driven Cavity," NASA-SP-378, pp. 47-59, 1975.

APPENDIX A

The differential equation system modelling the incompressible flow is

$$u,t + uu,x + uu,y = -\frac{1}{\rho} p,x + \nu(\nabla^2 u)$$

$$v,t + vv,x + vv,y = -\frac{1}{\rho} p,y + \nu(\nabla^2 v) \qquad \text{(A1)}$$

$$p,t + p(u,x) + p(v,y) = 0$$

The artificial time constant K is implicit in the time derivative p_t. We shall take the simplified form letting the viscous terms be absent for analysis. Rewriting (A1) in matrix form

$$\begin{pmatrix} u \\ v \\ p \end{pmatrix}_t + \begin{bmatrix} u & 0 & 1 \\ 0 & u & 0 \\ p & 0 & 0 \end{bmatrix} \begin{pmatrix} u \\ v \\ p \end{pmatrix}_x + \begin{bmatrix} v & 0 & 0 \\ 0 & v & 1 \\ 0 & p & 0 \end{bmatrix} \begin{pmatrix} u \\ v \\ p \end{pmatrix}_y = 0 \qquad \text{(A2)}$$

The character of equation (A2) can be studied from the property of the associated matrices letting

$$A = \begin{bmatrix} u & 0 & 1 \\ 0 & u & 0 \\ p & 0 & 0 \end{bmatrix} \quad \text{and} \quad B = \begin{bmatrix} v & 0 & 0 \\ 0 & v & 1 \\ 0 & p & 0 \end{bmatrix} \qquad \text{(A3)}$$

it is well known that the equation system (A2) is purely hyperbolic if the matrix

$$aA + bB \ ,$$

where a and b are arbitrary numbers has real distinct eigenvalues i.e., if the matrix

$$\begin{pmatrix} au + bv & 0 & s \\ 0 & au + bv & b \\ ap & bp & 0 \end{pmatrix} \tag{A4}$$

has distinct eigenvalues.

The eigenvalues of (A4) are

$$\lambda_1 = au + bv$$

$$\lambda_2 = \frac{au + bv}{2} + \frac{1}{2}\sqrt{(au + bv)^2 + 4(a^2 + b^2)p} \tag{A5}$$

$$\lambda_3 = \frac{au + bv}{2} - \frac{1}{2}\sqrt{(au + bv)^2 + 4(a^2 + b^2)p}$$

For $p > 0$ we find that for any arbitrary a, b eigenvalues are real and distinct. Another consequence of equation system (A2) is that there need not be any boundary conditions on p: i.e., the pressure is continuously dependent on u and v. This is rather fortuitous because the pressure equation that needs to be solved is a Poisson type equation which exhibits a great deal of dependence on the boundary conditions.

The presence of the artificial time multiplier K does not alter the conclusion made above. However the convergence rate of the solutions is affected drastically by the value of K.

APPENDIX B

BASIS FUNCTIONS FOR T-10 ELEMENTS

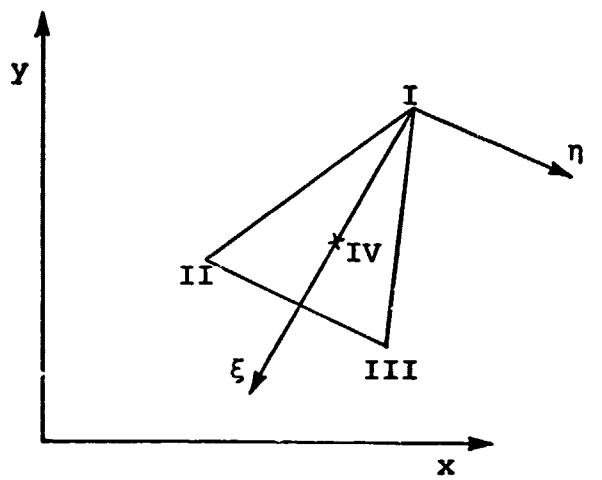

Figure B1.

A typical finite element is shown in Figure B1. The nodes I, II, III, IV have coordinates (x_I, y_I); (x_{II}, y_{II}), (x_{III}, y_{III}) and $\frac{x_I + x_{II} + x_{III}}{3}$, $\frac{y_I + y_{II} + y_{III}}{3}$ respectively with a reference x-y axis.

The transformation,

$$x = x_I + \frac{x_{II} + x_{III} - 2x_I}{2}\,\xi + \frac{x_{III} - x_{II}}{2}\,\eta$$

$$y = y_I + \frac{y_{II} + y_{III} - 2y_I}{2}\,\xi + \frac{y_{III} - y_{II}}{2}\,\eta \qquad \text{(B1)}$$

leaves the triangle with $\xi - \eta$ origin at node I and coordinates in the transformed plane of II, III and IV as (1, -1); (1, +1); (2/3, 0) respectively.

The basis functions ϕ_I, ϕ_{II}, ϕ_{III} can now be determined by requiring that

$$\phi_I = \phi_{II},\xi = \phi_{III},\eta = 1 \quad \text{at node I}$$

$$\phi_I = \phi_{II} = \phi_{III} = 0 \quad \text{at II, III and IV}$$

(B2)

$$\phi_I,\xi = \phi_{II},\xi = \phi_{III},\xi = \phi_I,\eta = \phi_{II},\eta = \phi_{III},\eta = 0 \quad \text{at II and III}$$

$$\phi_I,\xi = \phi_I,\eta = \phi_{II} = \phi_{II},\eta = \phi_{III} = \phi_{III},\xi = 0 \quad \text{at I}$$

or using a total of 30 algebraic equations (The basis functions ϕ_I, ϕ_{II}, ϕ_{III} are attached to node I such that $\phi_I = 1 = \phi_{II},\xi = \phi_{III},\eta$ at I.) Thus convection on the line

$$\phi_I = (1 - \xi)\left[1 + \xi - \frac{\xi^2}{4} - \frac{7}{4}\eta^2\right]$$

$$\phi_{II} = (1 - \xi)\left[\xi - \frac{3}{2}\xi^2 + \frac{\eta^2}{2}\right]$$

$$\phi_{III} = \eta(1 - \xi^2)$$

By rotating the cyclic order in figure B1 the "standard" triangles are produced with origins at II and III to obtain ϕ_{IV} to ϕ_{IX}. The expression for ϕ_X is as follows :

$$\phi_X = \frac{27}{4}(1 - \xi)(\xi^2 - \eta^2) .$$

APPENDIX C

DERIVATION OF STIFFNESS MATRIX AND LOAD VECTOR

Elsewhere, equation (12) summarized the results of Galerkin minimization of the residuals (equation (8), pages 6 and 7). We develop these results in the present sections.

Equation (8a), page 6, is reproduced below;

$$L_1(u^*) = 1 + \tau u^n D_x + \tau v^n D_y - \frac{\tau}{R}(D_{xx} + D_{yy}) \quad u^*$$

$$- \quad 1 - \tau u^n D_x - \tau v^n D_y + \frac{\tau}{R}(D_{xx} + D_{yy}) \quad u^{n-1}$$

$$+ D_x p^n (2\tau) \qquad \text{(C1)}$$

Figure C1 shows a typical triangulation of a domain Ω; the boundary Γ of Ω is singly connected.

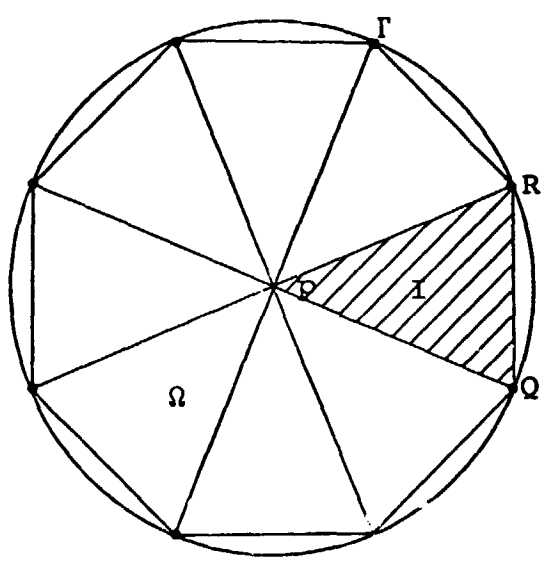

Figure C1.

Consider a triangulation PQR of Ω (shown hatched in above figure).

The shape functions ϕ_J have support only on this triangulation. We write

$$u^* = \phi^T\{u\}$$

$$v^* = \phi^T\{v\} \qquad \text{(C2)}$$

$$p^* = \phi^T\{p\}$$

where u, v, p are the nodal variables. The Galerkin technique applied to equation (C1) yields

$$\iint_\Omega L_1\phi_J d\Omega = 0 \qquad J = 1, 2, \ldots 10 \qquad \text{(C3)}$$

a total of 10 equations.

The known fields at time steps (n) and (n - 1) can be expanded in the form similar to equation (C1) yields

$$u^n = \phi^T u^n = \sum_k \phi_k u_k^n$$

$$v^{n-1} = \phi^T v^{n-1} = \sum_k \phi_k v_k^{n-1} \qquad \text{(C4)}$$

We also note that

$$D_x u = D_x \phi^T u = \Sigma \phi_{j,x} u_j \qquad \text{(C5)}$$

Applying the integral condition equation (C3) to equation (C1) the following relation is obtained:

$$\iint_\Omega \left[1 + \tau \langle\phi_k u_k^n\rangle D_x + \langle\phi_k v_k^n\rangle D_y - \frac{\tau}{R}\left(D_{xx} + D_{yy}\right)\right] u^* \phi_j d\Omega$$

$$= \iint_\Omega \left[1 - \tau \langle\phi_k u_k^n\rangle D_x \tau \langle\phi_k v_k^n\rangle D_y + \frac{\tau}{R}\left(D_{xx} + D_{yy}\right)\right] u^{n-1}\phi_j d\Omega$$

$$- 2\tau \iint_\Omega D_x p^n \phi_j d\Omega \qquad \text{(C6)}$$

$$j = 1, 2, \ldots 10$$

The right hand side of equation system (C6) consists of known functions and hence gives rise to the load vector. The left hand side of (C6) is an algebraic expression in the nodal variables u.

The equation system (C6) can be summarized as

$$\Sigma A_{ij} u_i = b_j \quad , \quad j = 1, 2 \ldots 10 \tag{C7}$$

where

$$A_{ij} = \iint_{\Omega} \left[\phi_i \phi_j + \tau \langle \phi_k u_k^n \rangle \phi_{i,x} \phi_j + \langle \phi_k v_k^h \rangle \phi_{i,y} \phi_j \right.$$
$$\left. - \frac{\tau}{R} \left(\frac{\partial}{\partial x} \phi_{i,x} \right) \phi_j + \left(\frac{\partial}{\partial y} \phi_{i,y} \right) \phi_j \right] d\Omega \tag{C8}$$

Due to the nature of the finite element that we chose, (piecewise continuous first derivatives across interelement boundaries) we apply Green's theorem to modify the last two terms in right hand side of equation (C8), which is stated below,

$$\iint_{\Omega} \nabla x \vec{F} d\Omega = \int_{\Gamma} E n d\vec{s} \tag{C9}$$

Thus, equation (C8) modifies to

$$A_{ij} = \iint_{\Omega} \phi_i \phi_j d\Omega + \tau \iint_{\Omega} \sum_k \left\{ \langle \phi_k u_k^n \rangle \phi_{i,x} \phi_j + \langle \phi_k v_k^n \rangle \phi_{i,y} \phi_j \right\} d\Omega$$
$$+ \frac{\tau}{R} \iint_{\Omega} \left\{ \phi_{i,x} \phi_{j,x} + \phi_{i,y} \phi_{j,y} \right\} d\Omega$$
$$- \frac{\tau}{R} \int_{\Gamma} \left\{ \phi_j \phi_{i,x} dy - \phi_j \phi_{i,y} dx \right\} \tag{C10}$$

The weak form of Galerkin minimization procedure enables us to order the element connectivity such that the boundary integrals cancel out for all interior nodes. Only for boundary nodes need the boundary integrations be carried out. Similar relation as (C10) can be found for b_j.